AIAA JOURNAL
Vol. 36, No. 7, July 1998

Technical Notes

TECHNICAL NOTES are short manuscripts describing new developments or important results of a preliminary nature. These Notes cannot exceed 6 manuscript pages and 3 figures; a page of text may be substituted for a figure and vice versa. After informal review by the editors, they may be published within a few months of the date of receipt. Style requirements are the same as for regular contributions (see inside back cover).

Method for Generating Equilibrium Swirling Inflow Conditions

Charles D. Pierce* and Parviz Moin†
Stanford University, Stanford, California 94305

I. Introduction

SWIRLING flows are used extensively in engineering applications, in particular, for flame stabilization in the combustor of gas-turbine engines. Physically, swirl is generated by tangential jets or contoured or plane vanes, which are difficult to simulate numerically. As modern simulation and experimental methods allow for more detailed characterization of flow behavior, it has become increasingly important to provide well-defined, reproducible inlet conditions. This problem has not been previously addressed for swirling flows. Several experiments have been done in idealized combustor geometries, but most did not use idealized inflow conditions, partially negating the benefits of using an idealized geometry.

Computation of turbulent swirling flows has been carried out mostly in the Reynolds-averaged turbulent flow prediction context. There, the inflow condition is usually determined by specifying either experimental data or simple algebraic mean profiles. Further discussion is provided in a review paper by Sloan et al.[1] The present study appears to be the first attempt at large eddy simulation of turbulent swirling flows. The azimuthal body force technique, described here, represents a means of predicting, rather than prescribing, swirling inflow boundary conditions.

II. Equilibrium Swirl and the Azimuthal Body Force

The problem of numerical generation of swirl is related to the larger issue of specifying inflow boundary conditions. For simulations and analyses, well-defined, fully developed conditions are usually preferred, whereas practical devices often involve complicated hardware (such as tangential jets or swirl vanes) that is difficult to model directly. However, as swirling flows are not self-sustaining, they must eventually decay toward equilibrium, independent of the form of the initial forcing that created them. If this relaxation process is sufficiently fast or if the forcing device is located sufficiently far upstream, then an equilibrium swirling inflow condition that is easier to model will result. This is also the closest flow to a fully developed swirling flow.

Because of its simplicity and reproducibility, equilibrium swirl should become a standard inflow condition for models and fundamental experiments. Although an equilibrium inflow condition will not handle all cases, it does represent a logical, idealized starting point. Indeed, practical swirling flows may be far from equilibrium, requiring detailed computation of the actual swirl-generating mechanism or a far more complex modeling procedure for their accurate description. In this case, the assumption of equilibrium inflow conditions represents only a first-order approximation.

A simple method for generating equilibrium swirling flows numerically is to solve for the flow driven by fictitious axial and azimuthal body forces in a spatially periodic section, from which data are fed as the inflow boundary condition into the main computational domain. The axial body force represents the mean pressure gradient that drives the physical flow and has long been established as a means of driving spatially periodic pipe and channel flows. On the other hand, the azimuthal body force used to drive the swirl component is not physically producible and should be thought of as existing only to overcome drag from the walls. The resulting flow is a stationary approximation to slowly decaying swirl.

III. Choosing the Forcing Profile

Consider the steady swirling flow in a long pipe of radius R. We examine the effect of different body forces in the azimuthal momentum equation on the velocity profiles. For stationary, axisymmetric, parallel flow, the axial and azimuthal momentum equations with body forces reduce to

$$\frac{1}{r}\frac{\mathrm{d}}{\mathrm{d}r}(r\tau_{xr}) + f_x = 0, \qquad \frac{1}{r}\frac{\mathrm{d}}{\mathrm{d}r}(r\tau_{r\theta}) + \frac{\tau_{r\theta}}{r} + f_\theta = 0 \quad (1)$$

where the total shear stresses τ_{xr} and $\tau_{r\theta}$ include both viscous and turbulent contributions. Note that the axial and azimuthal equations (1) are coupled only through the turbulent stresses. The radial profile of the axial body force $f_x(r)$ is taken to be uniform as in the Poiseuille flow. For the swirling case, there does not exist a corresponding physical mechanism for driving the flow, and so there is some freedom in choosing the forcing profile $f_\theta(r)$. Figure 1a compares mean azimuthal (swirl) velocity profiles obtained from large eddy simulation of purely swirling turbulent pipe flow (zero mean axial flow) using constant, linear, and quadratic profiles for f_θ:

$$f_\theta(r) = F, \qquad F(r/R), \qquad F[1 - 4(r/R - 1/2)^2] \quad (2)$$

where F is a constant scaling factor that determines the overall strength of the applied force. Note that the velocity profiles in Fig. 1 are normalized to have the same wall shear stress and that the resulting swirl velocity profiles are rather insensitive to large changes in the forcing profile used, especially near solid boundaries.

The more common case is that of swirling annular flow. This flow has also been tested with various azimuthal body force profiles. Again, for purely swirling flow, results are presented in Fig. 1b for uniform, linear, and inverse-r profiles:

$$f_\theta(r) = F, \qquad F(r/R), \qquad F(R/r) \quad (3)$$

where R is the radius of the outer wall of the annulus. Again note that the results are rather insensitive to the forcing profile shape and more so when the flow is bounded by walls. A uniform body force appears to be adequate, and for simplicity, it was chosen for use in all subsequent simulations. The Reynolds number, based on pipe radius and shear velocity in Fig. 1a and based on annulus half-width and inner–outer wall average shear velocity in Fig. 1b, was 1.8×10^2, which is the Reynolds number used in Ref. 2.

Experience has shown that the desired swirl number, which is the ratio of the axial fluxes of angular and axial momentum divided by overall radius,

$$S = \frac{\int \overline{(\rho u w)} r^2 \,\mathrm{d}r\,\mathrm{d}\theta}{R \int \overline{(\rho u^2)} r \,\mathrm{d}r\,\mathrm{d}\theta} \quad (4)$$

is easy to achieve by adjusting the strength of the body force.

Received Sept. 18, 1997; revision received March 25, 1998; accepted for publication April 5, 1998.

*Research Assistant, Department of Mechanical Engineering.
†Professor, Departments of Mechanical Engineering and Aeronautics and Astronautics.

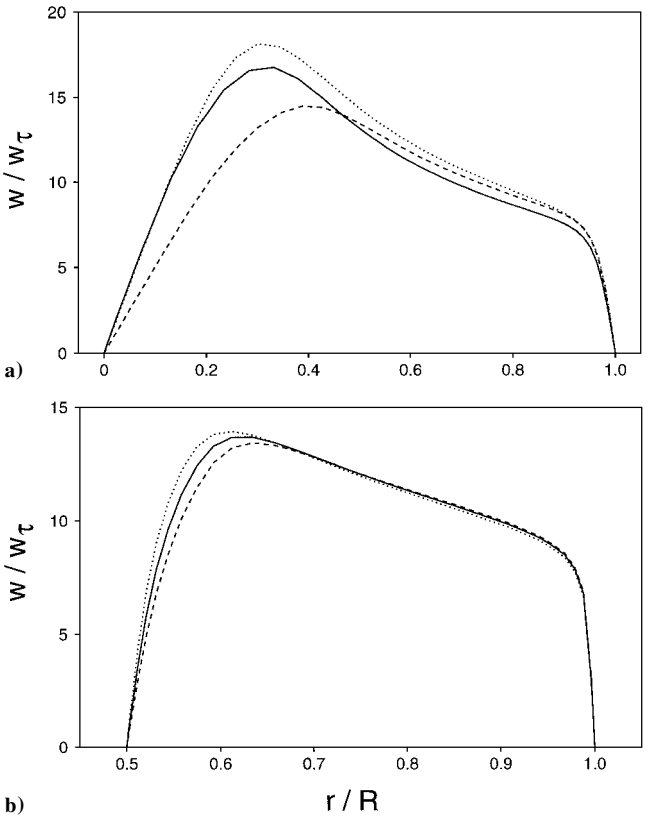

Fig. 1 Effect of azimuthal body force distribution on mean swirl velocity profiles in a) purely swirling turbulent pipe flow (——, constant; - - - -, linear; and · · · · · ·, quadratic) and b) purely swirling turbulent flow in an annulus (——, constant; - - - -, linear; and · · · · · ·, inverse-*r*).

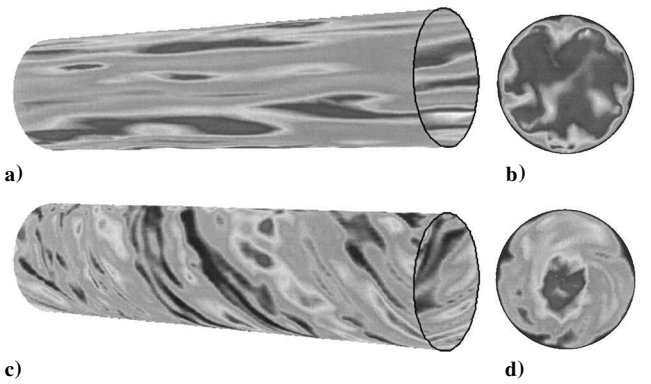

Fig. 2 Shades of gray (originally color), representing varying values of axial velocity, reveal flow structure: a) and b) nonswirling turbulent pipe flow, $Re_\tau = 1.8 \times 10^2$; c) and d) swirling turbulent pipe flow, $Re_{\tau,x} = Re_{\tau,\theta} = 1.8 \times 10^2$; a) and c) cylindrical surfaces in the near-wall region; and b) and d) end views.

For the case of swirling pipe flow driven by constant f_θ and combined with axially driven flow, a graphical representation of the axial velocity is shown in Figs. 2c and 2d. For comparison, nonswirling turbulent pipe flow is depicted in Figs. 2a and 2b. In Fig. 2a, high- and low-speed streaks, oriented along the flow direction, are visible. In the end view, Fig. 2b, ejections of low-speed fluid from the wall can be seen as mushroom-like structures protruding from the wall layer. In Fig. 2c, the wall streaks form helical patterns that are aligned with the local flow direction. And in Fig. 2d, the vortex core is indicated by a large, circular blob structure. This is a region of reduced turbulence level and increased axial and azimuthal velocity due to the stabilizing effect of rotation.

IV. Validation

We have used this method to generate inflow conditions for large eddy simulations of a confined coaxial jet (Fig. 3), an idealized gas-turbine combustor geometry. The large eddy simulations were performed using the dynamic model as described for nonswirling jets by Akselvoll and Moin.[3,4] Good agreement has been obtained with the experiment using a uniform azimuthal body force distribution, adjusted in strength to match the swirl number of the experiment. Figure 4 shows the swirl velocity profiles at axial stations near the expansion, which are compared with the experiments of Sommerfeld et al.[5] and Roback and Johnson.[6] The swirl number [defined by Eq. (4)] and Reynolds number (based on overall jet diameter and mass flow rate) in the experiment of Sommerfeld et al.[5] were 0.47 and 5.2×10^4, respectively, and 0.41 and 8.0×10^4, respectively, in the experiment of Roback and Johnson.[6] The figures on the left show the data of Sommerfeld et al.[5] at an axial location of $x/R = 0.09$, and the figures on the right show the data of Roback and Johnson[6] at $x/R = 0.17$. The agreements of the computational results with both experiments are satisfactory, validating the effectiveness of the simple swirl generation method described in this Note.

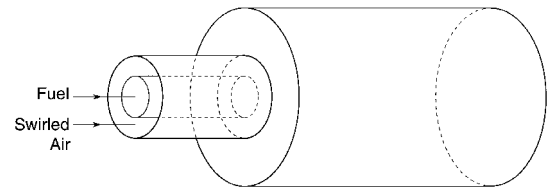

Fig. 3 Schematic of a coaxial jet combustor.

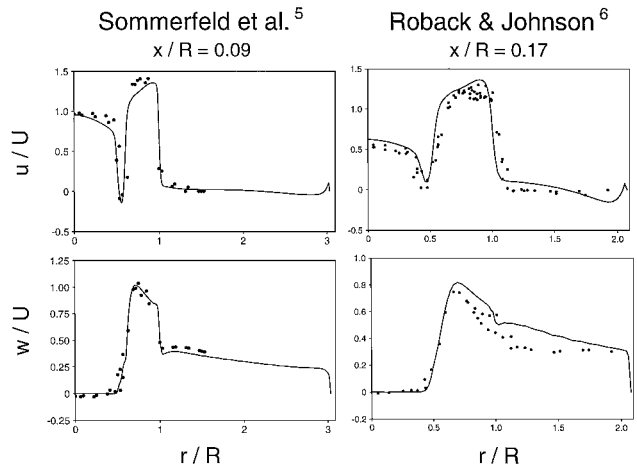

Fig. 4 Radial profiles of mean axial velocity (top) and azimuthal velocity (bottom) at the first axial station after the expansion: ——, large eddy simulation, and ●, experiment.

V. Conclusion

A method for generating inflow boundary conditions for numerical simulation of confined swirling flows was presented. Using an azimuthal body force, a stationary, axially homogeneous (equilibrium or fully developed) swirling flow was generated. This technique was used in large eddy simulation of a coaxial jet combustor. The results are in good agreement with the experimental data, establishing the fidelity of the method.

Acknowledgments

Support for this work was provided by the Air Force Office of Scientific Research under Grant F49620-95-1-0185. Computer time was provided by NASA Ames Research Center.

References

[1] Sloan, D. G., Smith, P. J., and Smoot, L. D., "Modeling of Swirl in Turbulent Flow Systems," *Progress in Energy and Combustion Science*, Vol. 12, No. 3, 1986, pp. 163–250.

[2] Kim, J., Moin, P., and Moser, R., "Turbulence Statistics in Fully Developed Channel Flow at Low Reynolds Number," *Journal of Fluid Mechanics*, Vol. 177, 1987, pp. 133–166.

[3] Akselvoll, K., and Moin, P., "An Efficient Method for Temporal Integration of the Navier–Stokes Equations in Confined Axisymmetric Geometries," *Journal of Computational Physics*, Vol. 125, No. 2, 1996, pp. 454–463.

[4]Akselvoll, K., and Moin, P., "Large-Eddy Simulation of Turbulent Confined Coannular Jets," *Journal of Fluid Mechanics*, Vol. 315, 1996, pp. 387–411.

[5]Sommerfeld, M., Ando, A., and Wennerberg, D., "Swirling, Particle-Laden Flows Through a Pipe Expansion," *Journal of Fluids Engineering*, Vol. 114, No. 4, 1992, pp. 648–656.

[6]Roback, R., and Johnson, B. V., "Mass and Momentum Turbulent Transport Experiments with Confined Swirling Coaxial Jets," NASA CR-168252, Aug. 1983.

K. Kailasanath
Associate Editor

Prediction of Shock Angles Caused by Sharp Delta Wings with Attack Angle

S. Koide*
Japan Defense Agency, Tokyo 154, Japan
and
A. F. Loria† and H. Babinsky‡
Cambridge University,
Cambridge CB2 1PZ, England, United Kingdom

Introduction

FOR glancing shock-wave/turbulent-boundary-layer interactions, the inviscid shock wave has an important role for specifying the interaction behavior regardless of the shape of the shock generator.[1] Hence, the trace of the shock wave on the wall provides an important reference position (the imaginary position that would exist if no boundary layer were presented on the wall) for understanding the interaction. The first author recently proposed empirical prediction methods for the shock angles caused by a series of rhombic delta wings (RDWs) at zero angle of attack[2] (Fig. 1a) and flat delta wings (FDWs) with angle of attack[3] (Fig. 1b). Using these methods, the shock angle on the plane of symmetry of the wing, β, can be predicted easily. This angle also specifies the trace of a shock wave along the wall when a swept sharp fin (the half-cut model of the RDW or FDW) is placed on the wall (equivalent to the position of the plane of symmetry for the wing). In this Note, the two methods are combined to predict the shock angles for sharp delta wings (SDWs) with angle of attack, in which both the RDWs and FDWs are included (Fig. 1c). Using the combined method, one can specify the trace of the shock generated by a swept sharp fin on the wall for various angles of attack α, sweep angles λ, half-apex angles ε, and Mach numbers M.

Summary of the Shock-Angle Prediction Methods for RDWs at Zero α and FDWs with α

For the RDWs at zero α, Ref. 2 suggested the following approach: The shock angles β_{RDW} obtained computationally and experimentally at various M, ε, and λ were nondimensionalized by the parameter $[\beta_{\mathrm{RDW}}/\beta_{\mathrm{OS}}(\varepsilon)] \cdot 2\zeta/(\pi M^a)$ and were plotted against $\zeta = \tan^{-1}[1/(\sin\varepsilon \tan\lambda)]$ (in radians; see Fig. 1a). In the parameter, the power a is $(\pi/2 - \zeta)/3$ and $\beta_{\mathrm{OS}}(\varepsilon)$ is the theoretical two-dimensional oblique shock angle for a flow deflection ε. To correlate the parameter against ζ, a fourth-order, least-squares equation was obtained:

$$F(\zeta) = -0.2504 + 0.8081\zeta - 0.1829\zeta^2 - 0.0971\zeta^3 + 0.1318\zeta^4 \tag{1}$$

Received Feb. 2, 1998; revision received March 10, 1998; accepted for publication March 25, 1998.

*Senior Research Engineer, Technical Department, Technical R&D Institute, 1-2-24 Ikejiri, Setagaya. Member AIAA.

†Mechanical Engineering Student, Department of Engineering, Trumpington Street.

‡Lecturer in Aerodynamics, Department of Engineering. Member AIAA.

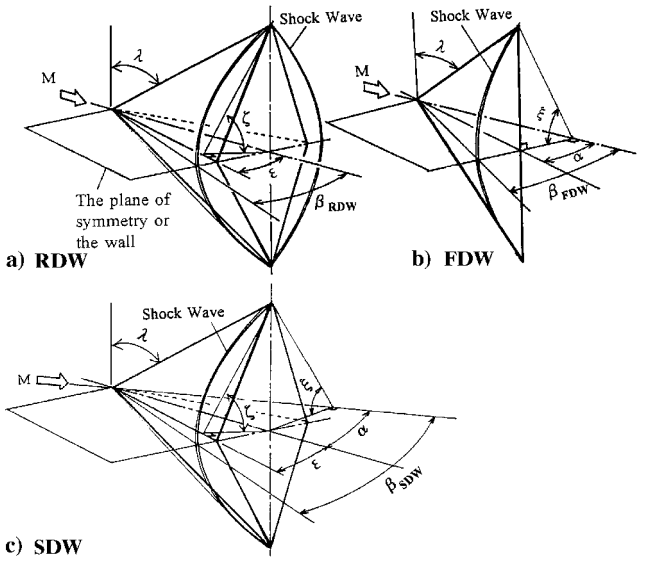

Fig. 1 Schematic views.

The value of β_{RDW} is then determined directly from

$$\beta_{\mathrm{RDW}} = \pi\beta_{\mathrm{OS}}(\varepsilon)F(\zeta)M^a \Big/ (2\zeta) \tag{2}$$

Similarly, the shock angle for the FDWs with α can be predicted by[3]

$$\beta_{\mathrm{FDW}} = \pi\beta_{\mathrm{OS}}(\alpha)G(\xi)M^b \Big/ (2\xi) \tag{3}$$

where ξ is $\tan^{-1}[1/(\sin\alpha \tan\lambda)]$ (in radians; see Fig. 1b), the power b is $(\pi/2 - \xi)/3$, and $G(\xi)$ has been chosen as

$$G(\xi) = -0.0202\xi + 1.0204\xi^2 - 0.8885\xi^3 + 0.3234\xi^4 \tag{4}$$

Prediction of the Shock Angles for SDWs with α

The shock angle for SDWs with angle of attack may be expressed by the combination of the two angles, i.e., $\beta_{\mathrm{SDW}} = f(\beta_{\mathrm{RDW}}, \beta_{\mathrm{FDW}})$. To construct a prediction method for β_{SDW}, one has to consider the following conditions. 1) When α approaches 0 deg, β_{SDW} has to approach β_{RDW}. 2) When ε approaches 0 deg, β_{SDW} has to approach β_{FDW}. 3) When λ approaches 0 deg, β_{SDW} has to approach $\beta_{\mathrm{OS}}(\alpha + \varepsilon)$ (see Fig. 1). To satisfy these conditions, the relationship

$$\beta_{\mathrm{SDW}} = \beta_{\mathrm{FDW}}\beta_{\mathrm{RDW}}\beta_{\mathrm{OS}}(\alpha + \varepsilon)/[\beta_{\mathrm{OS}}(\alpha)\beta_{\mathrm{OS}}(\varepsilon)] \tag{5}$$

has been introduced. It can be seen from Eqs. (2) and (3) that β_{RDW} and β_{FDW} become $\beta_{\mathrm{OS}}(\varepsilon)$ and $\beta_{\mathrm{OS}}(\alpha)$, respectively, when λ approaches 0 deg, and both of them become the Mach angle $[\mu = \sin^{-1}(1/M)]$ when ε and α approach 0 deg. Hence Eq. (5) satisfies conditions 1–3.

To check the validity of Eq. (5), parametric experiments have been carried out at Cambridge University's 21×11 cm^2 supersonic wind tunnel. Eight RDWs varying in sweep ($\lambda = 45$–73 deg) and half-apex angle ($\varepsilon = 6$–14 deg) were tested over three Mach numbers (1.8, 2.5, and 3.5 with an error of $\pm 1\%$), while the angle of attack was varied in 5-deg steps ($\alpha = 5$–20 deg). The shock angles were measured from shadowgraph images. The optical setup was adjusted to maximize the measurement accuracy. Nevertheless, an error of 2% of the angle was determined as an upper limit.

Figure 2 shows experimentally obtained values of β_{SDW} against angles predicted by Eq. (5). It can be seen that the agreement between experiment and prediction is very good; 80% of the predictions lie within 2 deg of the experimental values, and 50% are within 1 deg. However, some of the predicted values can be seen to depart from the solid line. Most of these are where $\lambda \geq 70$ deg at the lower Mach numbers of 1.8 and 2.5 (see the triangle points in Fig. 2). Under such conditions, the shock wave is nearly circular, and therefore the prediction using β_{OS} deteriorates. However, even for λ above 70 deg,